TECHNICAL NOTE

D-1088

RADIANT HEAT TRANSFER BETWEEN NONGRAY

PARALLEL PLATES OF TUNGSTEN

By J. Robert Branstetter

Lewis Research Center
Cleveland, Ohio

NATIONAL AERONAUTICS AND SPACE ADMINISTRATION

WASHINGTON   August 1961

NATIONAL AERONAUTICS AND SPACE ADMINISTRATION

TECHNICAL NOTE D-1088

RADIANT HEAT TRANSFER BETWEEN NONGRAY PARALLEL PLATES OF TUNGSTEN

By J. Robert Branstetter

SUMMARY

Net radiant heat flow between two infinite, parallel, tungsten plates was computed by summing the monochromatic energy exchange; the results are graphically presented as a function of the temperatures of the two surfaces. In general these fluxes range from approximately 8 to 25 percent greater than the results of gray-body computations based on the same emissivity data.

The selection of spectral emissivity data and the computational procedure are discussed. The present analytical procedure is so arranged that, as spectral emissivity data for a material become available, these data can be readily introduced into the NASA data-reduction equipment, which has been programmed to compute the net heat flux for the particular geometry and basic assumptions cited in the text.

Nongray-body computational techniques for determining radiant heat flux appear practical provided the combination of select spectral emissivity data and the proper mechanized data-reduction equipment are brought to bear on the problem.

INTRODUCTION

The radiant heat exchange between two infinite, parallel plates of opaque material can be readily computed by assuming that both materials are gray bodies; that is, that their emissivity is dependent on surface temperature and not on the wavelength of the radiation. The more laborious method of summing the monochromatic energy exchange over all the wavelengths of significance, reported in reference 1, indicates that the gray-body method can yield sizable errors. For example, the gray-body method of computing the radiant heat transfer between infinite parallel plates of pure aluminum and Inconel over a wide range of temperature and temperature difference produced errors ranging from 2 to 29 percent.

In the present paper the nongray-body heat flow between two tungsten plates was computed on a data-processing machine using a finite difference formula. For any two given surface temperatures the net heat

flux was determined by summing the net monochromatic heat flux over about 400 increments of wavelength.

Tungsten was chosen for two reasons. Its radiant behavior has been studied more than that of any other material. It is a strong contender for use as cathode and anode surfaces in thermionic energy conversion devices. Such devices operate at high temperatures, where the parasitic loss due to radiant heat exchange can have a pronounced effect on cycle efficiency.

The hemispherical spectral emissivity data used in the heat-flux equation were obtained from several sources in an endeavor to arrive at the most accurate set of data obtainable at this time. Hemispherical-total-emissivity values were computed from these spectral data and are compared with the generally accepted values of total emissivity. The computed total-emissivity data were used to obtain gray-body flux rates, and the results are compared with the nongray-body results.

The calculation procedure used in this report is described in some detail. The sources, and modifications thereto, of the tungsten emissivity data are presented along with a table of the hemispherical spectral emissivity data that were put into the heat-transfer calculations. A table and a figure show the net heat exchange for a broad range of surface temperatures.

ANALYSIS

This section presents the basic assumptions included in the analysis, the derivation of equations, the sources and modifications to the emissivity data, and the computational procedure.

Assumptions and Conditions

The calculations for nongray-body heat exchange between two infinite, parallel, flat plates of opaque material incorporated the following five assumptions or conditions:

(1) The two plates are identical.

(2) Each surface is at a constant temperature, surface 1 possessing a higher temperature than surface 2.

(3) Each surface is a diffuse radiator.

(4) At a given temperature and wavelength the hemispherical spectral emissivity $\varepsilon_{\lambda,T}$ equals the hemispherical spectral absorptivity, $\alpha_{\lambda,T}$.

(5) A vacuum exists between the two plates.

Equations

The basic equation (eq. 31-157 of ref. 2) for determining the nongray-body net heat exchange in watts per square centimeter is

$$q_{ng} = \int_{\lambda=0}^{\lambda=\infty} \frac{d\lambda}{\left(\varepsilon_{\lambda,T_1}^{-1} + \varepsilon_{\lambda,T_2}^{-1} - 1\right)} \left(J_{\lambda,T_1} - J_{\lambda,T_2}\right) \tag{1}$$

where

$$J_{\lambda,T} = 37,404 \; \lambda^{-5} \left(e^{14,387/\lambda T} - 1\right)^{-1} \; w/(micron)(cm^2)$$

and $\left(\dfrac{1}{\varepsilon_{\lambda,T_1}^{-1} + \varepsilon_{\lambda,T_2}^{-1} - 1}\right)$ is the interchange factor. (Symbols are defined in the appendix.)

The equation written in finite difference form (assuming energy at wavelengths less than 0.2 micron as negligible and using the gray-body method at wavelengths greater than 20 microns) becomes

$$q_{ng} = \left[\sum_{\lambda=0.2}^{\lambda=20} \left(\frac{\Delta\lambda}{\varepsilon_{\lambda,T_1}^{-1} + \varepsilon_{\lambda,T_2}^{-1} - 1}\right)\left(J_{\lambda,T_1} - J_{\lambda,T_2}\right)\right] + \left(\frac{1}{\varepsilon_{20,T_1}^{-1} + \varepsilon_{20,T_2}^{-1} - 1}\right) \times$$

$$\left[\left(\sigma T_1^4 - \sum_{\lambda=0.2}^{\lambda=20} J_{\lambda,T_1} \Delta\lambda\right) - \left(\sigma T_2^4 - \sum_{\lambda=0.2}^{\lambda=20} J_{\lambda,T_2} \Delta\lambda\right)\right] \tag{2}$$

4

where $\sigma = 5.6699{\times}10^{-12}$ w/(sq cm)(${}^\circ$K^4), $\Delta\lambda = 0.05$ micron, and $\varepsilon_{20,T}$, the emissivity at 20 microns, is taken as the mean value of the emissivity for the bundle of energy at wavelengths greater than 20 microns.

The calculation of equation (2) requires that the spectral emissivity be provided at wavelengths of 0.2 to 20 microns in increments of 0.05 micron for temperatures T_1 and T_2.

The total hemispherical emissivity at the particular temperature ε_T is

$$\frac{\int_0^\infty \varepsilon_{\lambda,T} J_{\lambda,T}\, d\lambda}{\int_0^\infty J_{\lambda,T}\, d\lambda}$$

When expressed in finite difference form, this equation becomes

$$\varepsilon_T = \left[\left(\sum_{\lambda=0.2}^{\lambda=20} J_{\lambda,T}\,\varepsilon_{\lambda,T}\,\Delta\lambda \right) + \left(\sigma T^4 - \sum_{\lambda=0.2}^{\lambda=20} J_{\lambda,T}\,\Delta\lambda \right) \varepsilon_{20,T} \right] \div \sigma T^4 \quad (3)$$

where $\Delta\lambda = 0.05$ micron.

The equation used to determine the gray-body net-heat exchange is

$$q_g = \sigma \left(\frac{T_1^4 - T_2^4}{\varepsilon_{T_1}^{-1} + \varepsilon_{T*}^{-1} - 1} \right) \quad (4)$$

where the emissivity of the colder surface was evaluated at the geometric mean temperature

$$T* = \sqrt{T_1 \times T_2}$$

according to the empirical method of reference 3, and ε_T was obtained from a temperature-emissivity plot of the results by equation (3). These gray-body data (eq. (4)) are used herein for comparison purposes only.

Emissivity Data

Hemispherical spectral emissivity data for tungsten were obtained as follows:

Data at wavelengths less than 2.6 microns. - The normal spectral emissivity data obtained by DeVos (ref. 4) were selected for several reasons. Measurements were made over sizable ranges of temperature and wavelength. The quality of these data appeared very good. Emissivity values obtained from reference 4 data curves for temperatures of 1600°, 2200°, and 2800° K are shown in table I. The data were "corrected" in the following manner:

(a) Reduced $2\frac{1}{2}$ percent to correct for light scattering (ref. 5)

(b) Changed from normal to hemispherical by means of figure 1 (obtained from ref. 6)

(c) Linearly interpolated or extrapolated to temperatures of 1000°, 2000°, and 3000° K

(d) Linearly extrapolated from 2000° and 1000° K to 0° K and from 2000° and 3000° K to 4000° K (for reasons to be explained in the section Calculation Procedure).

Item (a) was suggested by Larrabee, whose carefully controlled experiments were limited to the visible spectrum. His results (ref. 5) show good agreement with the results of reference 4.

Converting the normal data to hemispherical data required only a small correction (fig. 1), since most of the emissivity values (table I) were reasonably large. Nevertheless, two types of checks were made on the validity of the conversion curve. Reference 5 presents spectral emissivity data at angles of incidence from 0° to 90° for a wavelength of 0.665 micron. An algebraic integration of these data over a hemisphere yielded the data point shown in figure 1. The other check was to compute $\varepsilon_{\lambda,T}$ and $\varepsilon_{\lambda,T,n}$ using the self-consistent electromagnetic wave equations in reference 6. Admittedly, both equations, while reasonably good at the longer wavelengths, yield inaccurate spectral emissivity values at the shorter infrared wavelengths of interest. Nevertheless, since the equations for $\varepsilon_{\lambda,T}$ and $\varepsilon_{\lambda,T,n}$ were self-consistent, it was felt that they would be indicative of the validity of the conversion curve as applied to the spectral data for tungsten. Calculations were made at 2000° and 3000° K (over a range of wavelength from 1 to 2.5 microns). Results, not shown, were in excellent agreement with the curve.

Since $\varepsilon_{\lambda,T}$ varies appreciably with temperature at most wavelengths of interest, it is fortunate that a nearly linear relation

exists between $\varepsilon_{\lambda,T}$ and temperature (table I). Hence, linear interpolation and extrapolation of these data to temperatures of $1000°$, $2000°$, and $3000°$ K appear well justified.

Data at wavelengths greater than 4 microns. - In this region experimental values of spectral emissivity were not found in the literature for broad bands of temperature and wavelength. Equations of Schmidt and Eckert (ref. 6) were considered to be as reliable as any other at long wavelengths for temperatures between $1000°$ and $3000°$ K. The procedure was as follows:

(a) Equations 4-84 and 4-85 of reference 6 were used to obtain the data for temperatures of $1000°$, $2000°$, and $3000°$ K (table II). The equations are:

For $0 < (r_T/\lambda)10^{-2} < 0.5$

$$\varepsilon_{\lambda,T} = 0.476 \sqrt{(r_T/\lambda)10^{-2}} - 0.148 \left(\frac{r_T}{\lambda}\right) \times 10^{-2} \tag{5a}$$

For $0.5 < (r_T/\lambda)10^{-2} < 2.5$

$$\varepsilon_{\lambda,T} = 0.442 \sqrt{(r_T/\lambda)10^{-2}} - 0.0995\left(\frac{r_T}{\lambda}\right) \times 10^{-2} \tag{5b}$$

Data for the electrical resistivity r_T were obtained from references 7 and 8.

(b) Then these data were linearly extrapolated to $0°$ and $4000°$ K in the manner described for the short-wavelength data.

Data at wavelengths between 2.6 and 4 microns. - The $\varepsilon_{\lambda,T}$ values were selected by plotting the previously described two sets of data (fig. 2) and joining them by a smoothly faired curve.

Surface properties. - To describe the surface properties of the metal represented by the emissivity data used in this report would be to toy somewhat with fancy. Yet some sort of a statement is called for if the heat-flux data are to be of engineering value. Data at the long wavelengths were for a "smooth" surface. Perusal of figure 3 will show that, at a temperature above $2000°$ K, more than half the energy exchange will be at the shorter wavelengths where data of reference 4 apply. DeVos painstakingly defined the pertinent properties of the rolled strip. Briefly stated, the tungsten was of high purity and was properly outgased and then annealed to ensure that no systematic changes in emissivity would occur after the annealing process. The final crystalline texture showed the crystal grains to be of the order of 30 microns and the surface to be predominately of the (100) plane.

Calculation Procedure

The requirement of a small wavelength interval $\Delta\lambda$ in order to obtain a good precision of results makes automatic data-processing equipment a practical necessity. The program used herein was so arranged that the equations to be solved were placed on one input and the tungsten emissivity data were placed on another. With the computation program arranged in this manner, little effort is required to change the spectral data input, and therefore the program is useful for computing the heat flux of other materials as spectral emissivity data become more plentiful. (The present program does not require that both surfaces be of the same material.)

Size of wavelength interval. - The selection of a wavelength interval $\Delta\lambda$ equal to 0.05 micron was based on the Planckian energy distribution (see fig. 3). Even with this relatively small interval, as much as 3 percent of the black-body energy at 3000° K is contained in an interval. However, the interval selected appeared satisfactory, since there was no noticeable data scatter observed during the plotting of the results of equation (2). With an interval severalfold larger than the one used, precision of the results would have been compromised.

Cutting off the orderly summation at a wavelength of 20 microns was justified on the basis of figure 3. At 1000° K the black-body energy in the tail (see eq. (2)) is about 1.5 percent of the total energy. Furthermore, the spectral emissivity decreases with increasing wavelength.

Temperature input. - The temperatures selected for computation of q_{ng} by equation (2) were

T_1, °K	T_2, °K
4000	3800, 3600, 3400, . . . 600
3800	3600, 3400, 3200, . . . 600
3600	3400, 3200, 3000, . . . 600
↓	↓
800	600

Equation (4), used to obtain the total hemispherical emissivity, was evaluated at temperatures of 1000°, 2000°, 3000°, and 4000° K.

Emissivity input. - Tungsten emissivity data were obtained directly from tables I and II. These data, as introduced into the computing machine, are presented in table III. A linear interpolation procedure was used to obtain $\varepsilon_{\lambda,T}$ at the particular values of wavelength and temperature needed in equations (2) and (3).

The emissivity data were extrapolated to temperatures above 3000° K and below 1000° K (tables I and II) in order to obtain flux data over a wider range of temperatures than would have been possible otherwise. At temperatures between 3000° K and the melting point, the linear extrapolation of the 2000° to 3000° K data is reasonably well justified. At these high temperatures (short wavelength region, i.e., table I data) the spectral emissivity varies almost linearly with temperature. At the other temperature extreme, the error in spectral emissivity associated with the linear extrapolation of the 2000° to 1000° K data into the region below about 800° K could be appreciable. Hence, flux calculations were not made for values of T_1 lower than 800° K.

The selection of wavelengths for the data input, given in table III, followed no hard and fast rule; however, greatest weight was given to the emissivity data at the shorter wavelengths, since the majority of the radiant energy is emitted there (figs. 2 and 3).

RESULTS AND DISCUSSION

The nongray-body heat-transfer data obtained using equation (2) are presented in their entirety in table IV. Also, they are shown in graphical form in figure 4. There the lines of constant temperature T_1 are shown as dashed lines at all values of $T_1 - T_2$ that are outside the temperature framework of the table. Data at temperatures above the melting point are useful only insofar as they can facilitate interpolation of T_1 data near the melting point, which is shown in the figure.

Under the heading "Emissivity input" the possibility of a rather large error in spectral emissivity for low values of temperature is discussed. It is primarily for this reason that the curves of constant temperature T_1 in figure 4 are shown as dashed lines in the vicinity of T_2 equal to zero. The computed data (shown as the solid lines of constant T_1), when plotted as shown, lead one to believe the flux is almost constant for all values of T_2 less than 600° K. Very likely this is the case. But it should be pointed out that, while the energy emitted by the T_2 surface $\left(\int_0^\infty J_{\lambda,T_2} \varepsilon_{\lambda,T_2} \, d\lambda \right)$ is relatively small, the amount of energy the T_2 surface absorbs is determined in considerable measure by its spectral absorptivity. As a rough approximation this absorbed energy is $\int_0^\infty \left(J_{\lambda,T_1} \varepsilon_{\lambda,T_1} \right) \varepsilon_{\lambda,T_2} \, d\lambda$. For large values of T_1, the values of $\varepsilon_{\lambda,T_2}$ that have the greatest influence on the net

heat flux are those having short wavelengths (fig. 2). Unfortunately, the $\varepsilon_{\lambda,T_2}$ values in the low-temperature and short-wavelength region were subject to a large temperature extrapolation (table I). This example illustrates the caution that must be exercised when one uses heat-flux data based on a rather limited amount of spectral emissivity data.

In figure 5 hemispherical total emissivities computed from the hemispherical spectral data of table III by means of equation (3) are compared with the widely used data of reference 9. The comparison of emissivities (fig. 5) is not intended to show either set of data to be in error. Rather, it does show that both sets of data are in fair agreement and that gray-body heat-flux calculations made using either set of data would give similar results.

A comparison of the gray- and nongray-body methods of computing heat flux is given in figure 6. The emissivities used in the gray-body calculations were obtained from the curve shown faired through the four data points given in figure 5. There is very little data scatter observed in figure 6. This attests to the desirability of using small increments of wavelength $\Delta\lambda$ in making radiant-heat-flux calculations by means of finite difference formulas. In all cases, the nongray-body flux is shown to be greater than the gray-body flux. In general, the discrepancy increased as T_1 was reduced and/or as $T_1 - T_2$ was increased. The minimum deviation occurred near the melting point and was approximately 8 percent. The maximum was about 25 percent. These results can be compared with the results obtained in reference 1 for Inconel, whose spectral emissivity was shown to decrease linearly with increasing wavelength. For most cases reported, the gray-body flux data ranged from 20 to 25 percent lower than the nongray-body flux.

SPECTRAL DATA ON OTHER MATERIALS

Reasonably accurate spectral emissivity data on high-temperature materials, although still greatly limited in quantity, are currently becoming available. It is most desirable that experimental data be obtained over the range of wavelengths necessary for heat-flux calculations. As an example, the data points in figure 2 are from an investigation (ref. 10) wherein normal spectral emissivity measurements were reported for a continuous band of wavelengths stretching from 0.45 to 12 microns. This reference shows that the variations of spectral emissivity with wavelength for tantalum and molybdenum are similar to that of tungsten. Hence, these two metals may exhibit a behavior not too much unlike that shown for tungsten in figure 6.

Spectral data such as these, when obtained over a wide range of temperature and for surfaces of well defined composition, will permit the computation of nongray-body flux data that are of greater accuracy than those obtainable by the gray-body method.

SUMMARY OF RESULTS

A comparison of the nongray- and gray-body methods of computing net heat flux between two infinite, parallel plates of tungsten shows:

1. Gray-body calculated flux was from approximately 8 to 25 percent too low. Errors similar to these have been observed elsewhere when the variation of spectral emissivity with wavelength is large.

2. Since many metals have a spectral emissivity - wavelength relation similar to that of tungsten, appreciable errors in the net heat flux between surfaces of these metals can be expected when gray-body calculation procedures are used.

3. Experimental apparatus has been perfected to the point where an ample amount of spectral emissivity data on many materials can be obtained with sufficient accuracy to justify using nongray-body techniques of computing net radiant heat flux.

4. The present analytical procedure is so arranged that, as spectral emissivity data for a material become available, these data can be readily introduced into the NASA data-reduction center which has been programmed to compute the net heat flux for the particular geometry and basic assumptions cited in the text.

CONCLUSION

The practicality of using nongray-body computational techniques to determine radiant heat flux appears most encouraging provided the combination of select spectral emissivity data and the proper mechanized data-reduction equipment are brought to bear on the problem.

Lewis Research Center
    National Aeronautics and Space Administration
        Cleveland, Ohio, June 15, 1961

E-1277

E-1277

APPENDIX - SYMBOLS

$J_{\lambda,T}$	Planck's distribution law equation, $w/(\text{micron})(\text{sq cm})$
q_g	net heat-transfer rate for gray-body conditions, $w/(\text{sq cm})$
q_{ng}	net heat-transfer rate for nongray-body conditions, $w/(\text{sq cm})$
r_T	electric resistivity, $(\text{microhm})(\text{cm})$
T	surface temperature, $^\circ K$
T^*	$\sqrt{T_1 \times T_2}$, $^\circ K$
α_T	hemispherical total absorptivity
$\alpha_{\lambda,T}$	hemispherical spectral absorptivity
ε_T	hemispherical total emissivity
$\varepsilon_{\lambda,T}$	hemispherical spectral emissivity
$\varepsilon_{\lambda,T,n}$	normal spectral emissivity
λ	wavelength, microns
σ	Stefan-Boltzmann constant, 5.6699×10^{-12} $w/(\text{sq cm})(^\circ K^4)$

Subscripts:

1	hotter surface
2	cooler surface

12

REFERENCES

1. Goodman, Stanley: Radiant-Heat Transfer Between Nongray Parallel Plates. Jour. Res. Nat. Bur. Standards, vol. 58, no. 1, Jan. 1957, pp. 37-40.

2. Jakob, Max: Heat Transfer. Vol. 2. John Wiley & Sons, Inc., 1957.

3. McAdams, W. K.: Heat Transmission. Third ed., McGraw-Hill Book Co., Inc., 1954.

4. DeVos, J. C.: A New Determination of the Emissivity of Tungsten Ribbon. Physica, vol. 20, 1954, pp. 690-714.

5. Larrabee, Robert Dean: The Spectral Emissivity and Optical Properties of Tungsten. Tech. Rep. 328, M.I.T., May 21, 1957.

6. Jakob, Max: Heat Transfer. Vol. 1. John Wiley & Sons., Inc., 1949.

7. Hampel, Clifford A., ed.: Rare Metals Hanibook. Reinhold Pub. Corp., 1954.

8. Anon.: Temperature - Its Measurement and Control in Science and Industry. Reinhold Pub. Corp., 1941.

9. Hodgman, Charles D., ed.: Handbook of Chemistry and Physics. Thirty-sixth ed., Chem. Rubber Pub. Co., 1954-1955.

10. Anon.: Measurement of Spectral and Total Emittance of Materials and Surfaces Under Simulated Space Conditions. Rep. PWA-1863, Pratt & Whitney Aircraft, 1960.

E-1277

TABLE I. - TUNGSTEN EMISSIVITY DATA BASED ON EXPERIMENT

Wave-length, λ, microns	Normal spectral emissivity (ref. 4), $\varepsilon_{\lambda,T,n}$			Hemispherical spectral emissivity, $\varepsilon_{\lambda,T}$							
	1600	2200	2800	1600 (a)	2200 (a)	2800 (a)	1000 (b)	2000	3000 (b)	0 (b)	4000 (b)
0.2	-----	-----	-----	0.4704	0.4594	0.4469	0.4815	0.4632	0.4426	0.4996	0.4218
.3	0.482	0.470	0.456	.4704	.4594	.4469	.4815	.4632	.4426	.4996	.4218
.4	.481	.470	.461	.4695	.4594	.4513	.4797	.4627	.4487	.4965	.4344
.5	.469	.458	.448	.4587	.4486	.4399	.4687	.4518	.4370	.4856	.4221
.6	.455	.444	.434	.4464	.4365	.4279	.4563	.4398	.4250	.4731	.4100
.7	.444	.432	.419	.4365	.4262	.4146	.4468	.4296	.4108	.4639	.3916
.8	.431	.414	.400	.4254	.4105	.3990	.4403	.4153	.3950	.4652	.3745
.9	.413	.396	.383	.4097	.3952	.3841	.4242	.4000	.3804	.4485	.3608
1.0	.390	.376	.367	.3900	.3786	.3710	.4015	.3824	.3685	.4205	.3545
1.1	.367	.358	.352	.3710	.3628	.3579	.3793	.3656	.3563	.3934	.3470
1.25	.331	.331	.331	.3404	.3404	.3404	.3404	.3404	.3404	.3404	.3404
1.4	.300	.307	.313	.3144	.3200	.3252	.3089	.3182	.3271	.2995	.3361
1.6	.263	.278	.292	.2822	.2952	.3075	.2696	.2910	.3116	.2477	.3322
1.8	.234	.255	.274	.2556	.2749	.2915	.2369	.2683	.2974	.2052	.3266
2.0	.210	.235	.259	.2335	.2567	.2784	.2103	.2492	.2857	.1710	.3223
2.2	.190	.218	.245	.2142	.2407	.2658	.1880	.2321	.2742	.1439	.3174
2.5	.170	.200	.229	.1943	.2238	.2512	.1655	.2141	.2610	.1169	.3087

Temperature, T, °K

aAlso corrected for light-scattering error.
bExtrapolated.

TABLE II. - TUNGSTEN EMISSIVITY DATA BASED

ON ELECTROMAGNETIC THEORY

Wave-length, λ, microns	Temperature, T, °K				
	1000	2000	˙3000	0 (a)	4000 (a)
	Hemispherical spectral emissivity, $\varepsilon_{\lambda,T}$				
4	0.112	0.163	0.1995	0.061	0.2355
5	.101	.147	.1815	.055	.216
6	.092	.136	.169	.0475	.2025
8	.081	.120	.149	.0425	.179
10	.0725	.1085	.135	.0365	.1615
12	.0675	.100	.123	.035	.146
16	.059	.0875	.110	.030	.132
20	.052	.077	.098	.027	.119

[a]Extrapolated.

TABLE III. - HEMISPHERICAL SPECTRAL

EMISSIVITY DATA FOR TUNGSTEN

Wave-length, λ, microns	Temperature, T, $^{\circ}$K		
	0	2000	4000
	Hemispherical spectral emissivity, $\varepsilon_{\lambda,T}$		
0.2	0.4996	0.4632	0.4218
.3	.4996	.4632	.4218
.4	.4965	.4628	.4344
.5	.4856	.4518	.4221
.6	.4731	.4398	.4100
.7	.4639	.4296	.3916
.8	.4652	.4153	.3745
.9	.4485	.4000	.3608
1.0	.4205	.3824	.3545
1.1	.3934	.3656	.3470
1.25	.3404	.3404	.3404
1.4	.2995	.3182	.3361
1.6	.2477	.2910	.3322
1.8	.2052	.2684	.3266
2.0	.1710	.2492	.3223
2.2	.1439	.2321	.3174
2.5	.1169	.2141	.3087
3.0	.0882	.1890	.2850
3.5	.0710	.1730	.2500
4.0	.0610	.1630	.2355
5.0	.0550	.1470	.2160
6.0	.0475	.1360	.2025
8.0	.0425	.1200	.1790
10.0	.0365	.1085	.1615
12.0	.0350	.1000	.1460
16.0	.0300	.0875	.1320
20.0	.0270	.0770	.1190

TABLE IV. - NONGRAY-BODY NET FLUX BETWEEN TWO INFINITE, PARALLEL PLATES OF TUNGSTEN

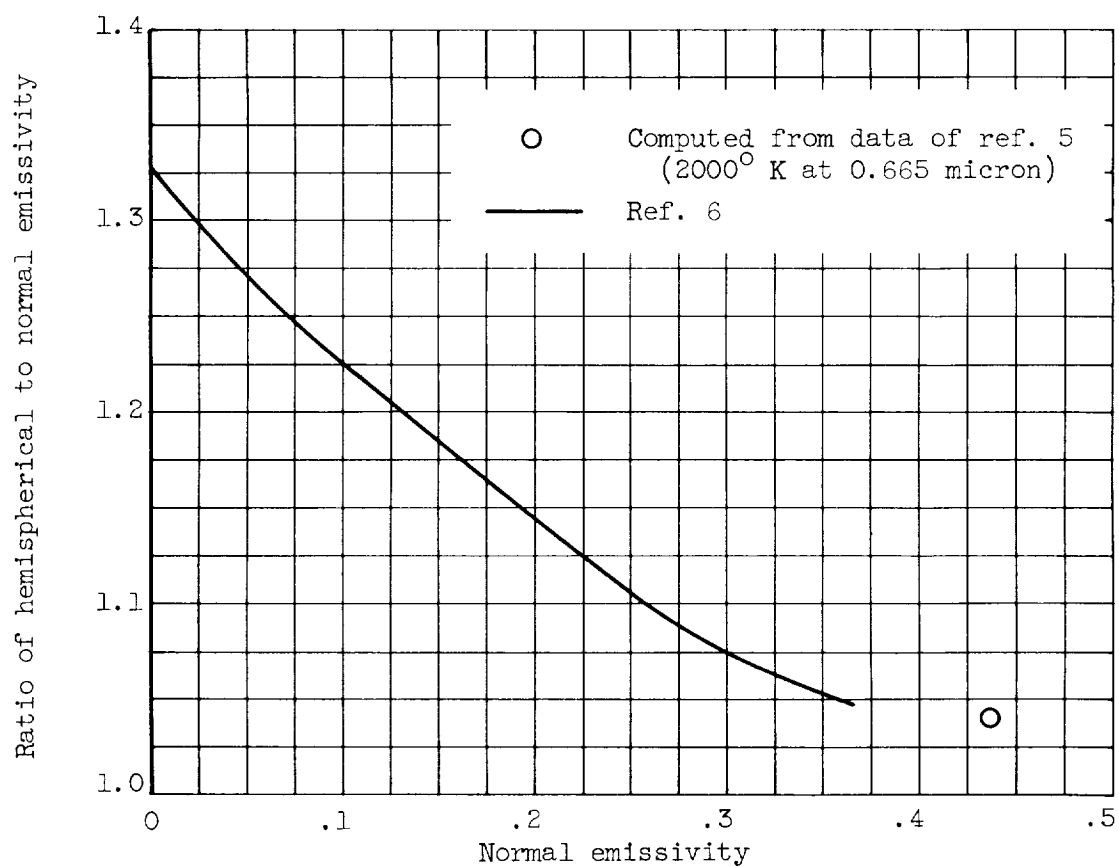| T_2, °K	Temperature, T_1, °K — Flux, w/sq cm																
	800	1000	1200	1400	1600	1800	2000	2200	2400	2600	2800	3000	3200	3400	3600	3800	4000
3800																	62.00
3600																52.45	114.5
3400															43.86	96.34	158.4
3200														36.20	80.09	132.6	194.8
3000													29.43	65.66	109.6	162.2	224.4
2800												23.51	52.96	69.21	133.2	185.9	248.2
2600											18.40	41.93	71.40	107.7	151.7	204.5	266.9
2400										14.06	32.47	56.00	85.50	121.8	165.9	218.8	281.4
2200									10.43	24.49	42.91	66.46	95.98	132.4	176.5	229.4	292.2
2000								7.476	17.91	31.97	50.38	73.94	103.5	139.9	184.1	237.1	300.0
1800							5.129	12.60	23.02	37.07	55.48	79.05	108.6	145.1	189.4	242.5	305.4
1600						3.332	8.452	15.90	26.30	40.34	58.74	82.30	111.9	148.4	192.7	245.9	309.0
1400					2.021	5.342	10.44	17.86	28.24	42.24	60.62	84.17	113.8	150.3	194.7	247.9	311.1
1200				1.124	3.134	6.432	11.50	18.88	29.21	43.19	61.52	85.06	114.6	151.2	195.6	248.9	312.2
1000			0.5583	1.671	3.659	6.925	11.95	19.29	29.56	43.48	61.79	85.28	114.8	151.4	195.8	249.2	312.6
800		0.2394	.7890	1.883	3.839	7.063	12.04	19.32	29.53	43.39	61.64	85.10	114.6	151.1	195.6	249.0	312.5
600	0.08421	.3176	.8523	1.920	3.840	7.015	11.93	19.14	29.30	43.09	61.29	84.69	114.2	150.7	195.2	248.6	312.1

Figure 1. - Ratio of hemispherical to normal emissivity of metallic surfaces. Suitable for either total or spectral emissivities of tungsten.
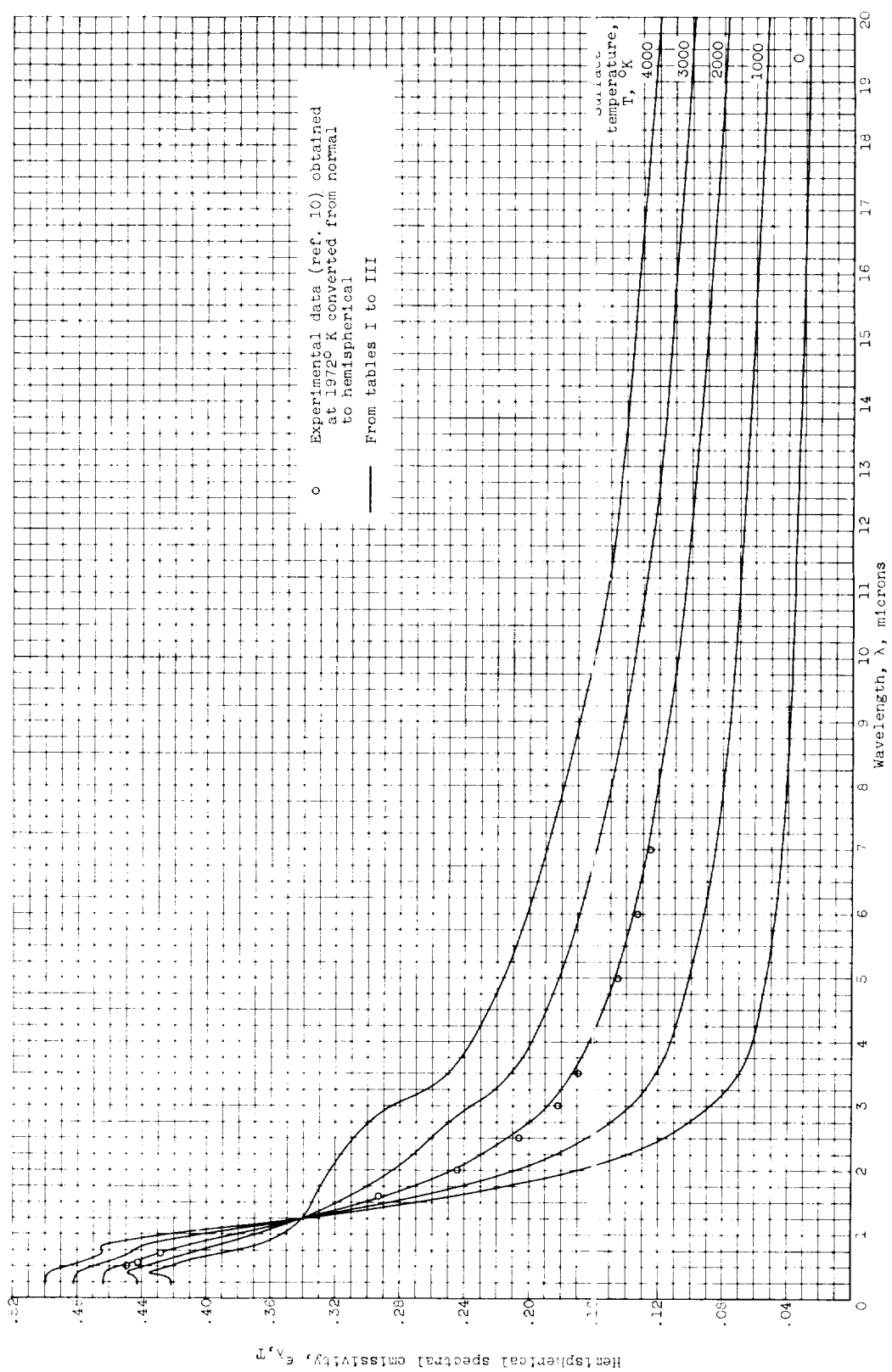
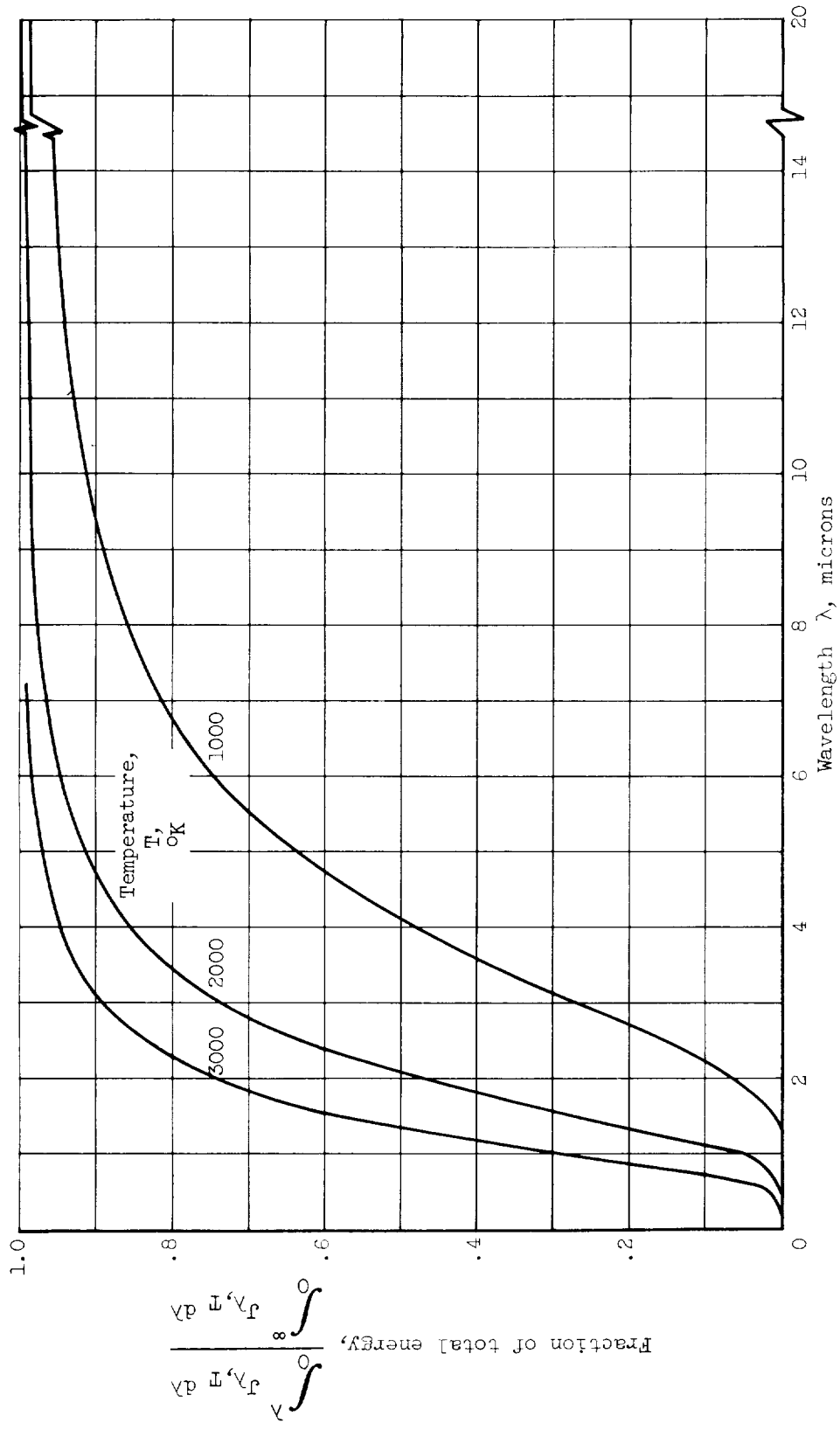Figure 2. - Spectral emissivity data for tungsten.

E-1277

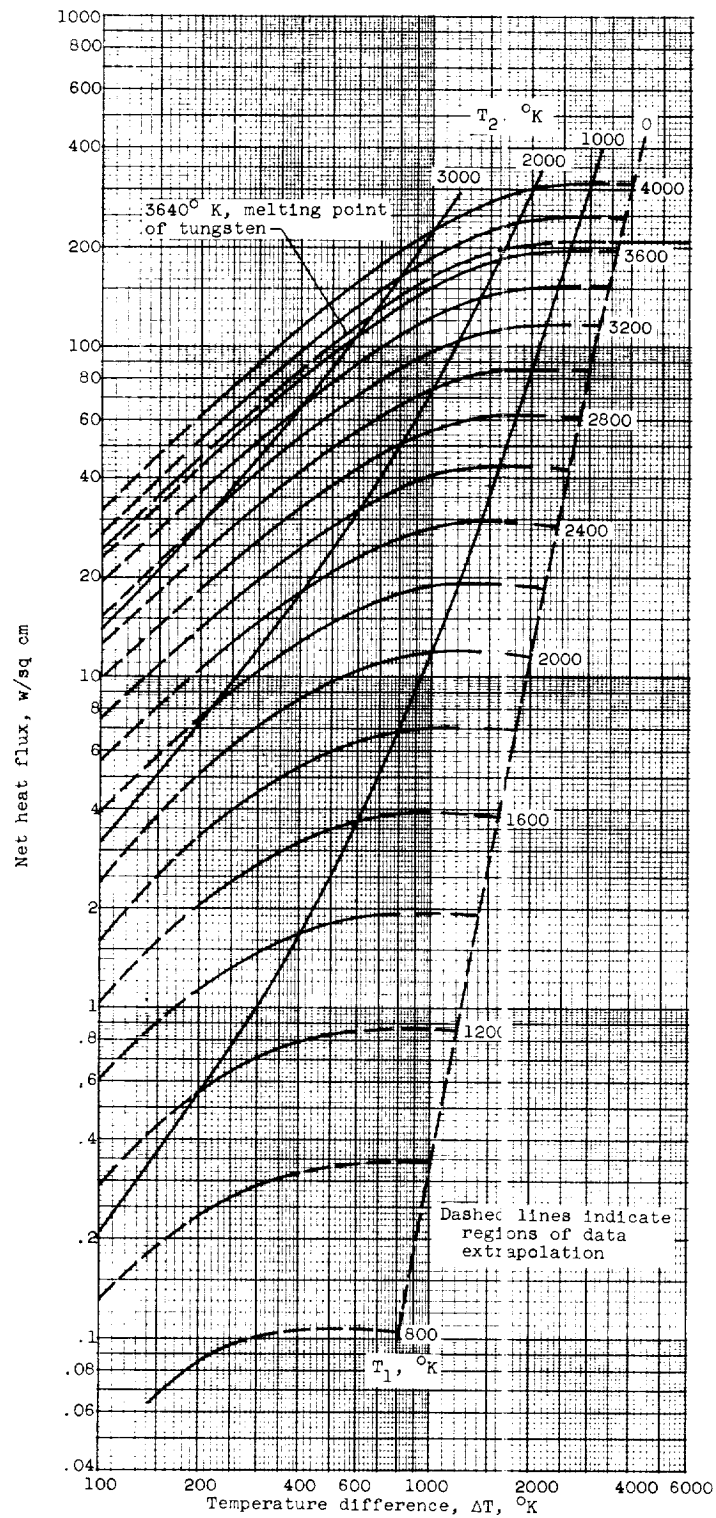Figure 3. - Spectral distribution of black-body energy.

E-1277

Figure 4. – Net radiant heat flux between two infinite,
parallel plates of tungsten. Surfaces approximately
those of straight-rolled strip that has been heat-
treated and annealed to ensure high purity and stable
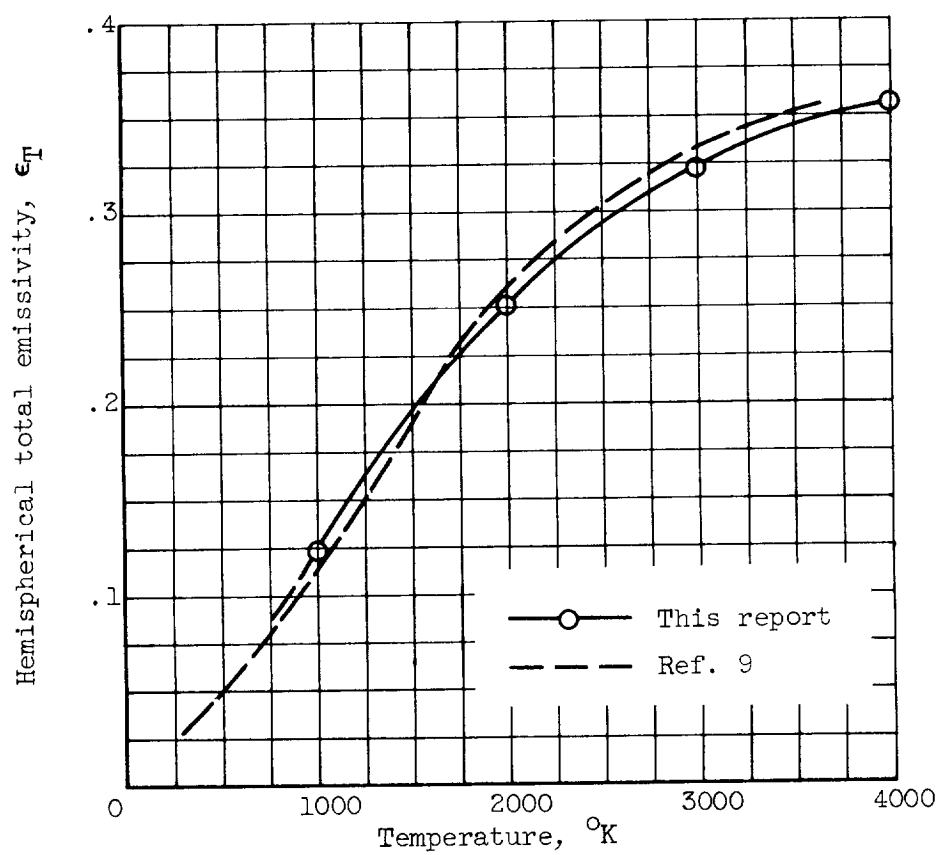crystalline structure.

E-1277

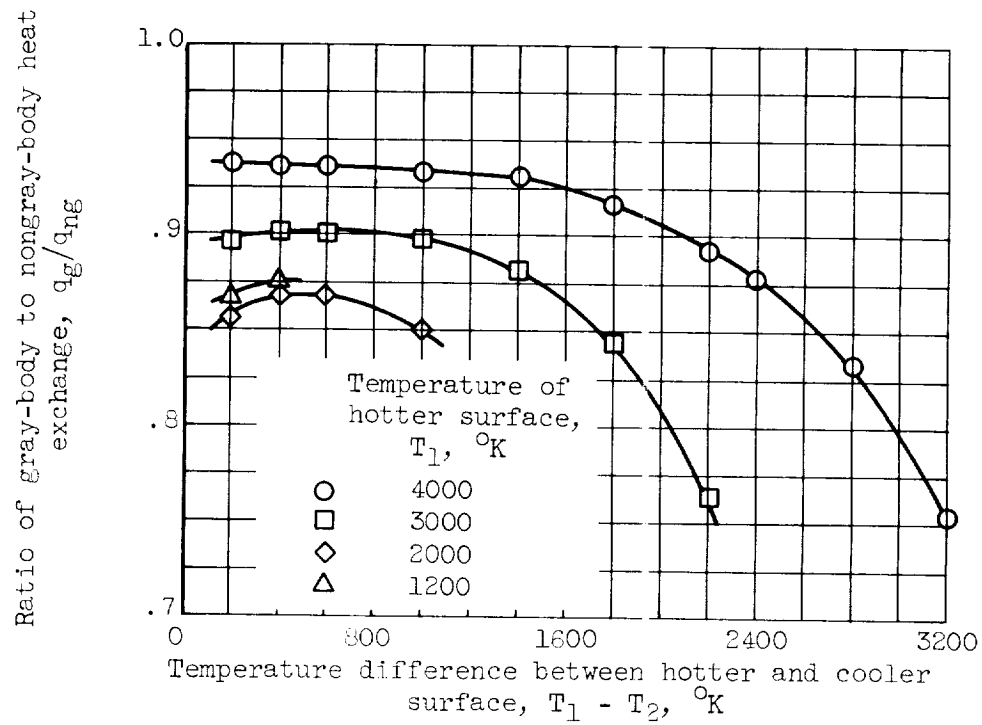Figure 5. - Comparison of hemispherical total emissivity data for tungsten.

Figure 6. - Comparison of gray- and nongray-body
methods for computing net heat flux between two
infinite, parallel plates of tungsten.